Research of Pattern Formation, edited by R. Takaki, pp. 377–387.

Mechanical Properties of Vertex Model for Two-Dimensional Random Cellular Structures

Kyozi KAWASAKI*, Tohru OKUZONO*, and Tatsuzo NAGAI**

**Department of Physics, Kyushu University 33, Fukuoka 812, Japan*
***Physics Department, Kyushu Kyoritsu University, Kitakyushu 807, Japan*

Abstract. Mechanical properties such as elasticity, plasticity and viscoelasticity of two-dimensional random cellular structure are studied by computer simulations of vertex models. We found that plasticity and hence hysterisis effects are intimately connected with topology changing processes of the cellular structure. The viscoelastic response of the system to externally applied uniform strain is also investigated and a scaling law in the stress-strain relationship is verified for small shear rates.

1. Introduction

Space-filling irregular cellular patterns form a class of random patterns most commonly found in nature as well as in various man-made materials (Weaire and Rivier, 1984). Their investigation is important not only for our understanding of some aspects of nature but also for better control of materials properties*. Knowing static and dynamics properties of elements constituting a cellular structure, we would like to develop statistical mechanics for dealing with systems consisting of large numbers of cells. Despite its importance, progress here has been rather limited so far. This is especially the case for highly disordered cellular patterns. These are strong correlations in the system imposed by the space-filling condition and no smallness parameter of expansion exists. Thus, up to now the most detailed knowledge of random cellular patterns was obtained by computer modelling. Here, one faces a dilemma of small system sizes for realistic simulation models and large

* See for instance New York Times, March 20, 1990.

system sizes for mutilated simulation models (Anderson and Rollett, 1990). Under such circumstances we have been studying properties of partially mutilated simulation models, the so-called vertex models, which still keep full topology of cellular structures (Nagai and Kawasaki, 1991). Our past studies, however, have focused on irreversible time evolution where cell boundaries are steadily reduced. In this article we report on our more recent studies on response of the system to external distortions whereby we hope to gain some insight into mechanical properties of cellular structures.

2. Vertex Model

The vertex models for cellular structures were described elsewhere (Nagai and Kawasaki, 1991) and here we only show the equation of motion of one such model (the model O') for two-dimension, which is the model actually employed in this work. The system consists of a set of vertices at $\boldsymbol{r}_i$, $i = 1, 2, \ldots$ which are intersections of three straight cell boundaries. Their velocities $\boldsymbol{v}_i$ are then given by

$$\boldsymbol{D}_i \cdot \boldsymbol{v}_i = -\sum_j^{(i)} \hat{\boldsymbol{r}}_{ij}, \tag{2-1}$$

where

$$\boldsymbol{D}_i \equiv \frac{1}{3L} \sum_j^{(i)} |\boldsymbol{r}_{ij}| \boldsymbol{n}_{\langle ij \rangle} \boldsymbol{n}_{\langle ij \rangle}. \tag{2-2}$$

Here L is a positive constant, $\boldsymbol{r}_{ij} \equiv \boldsymbol{r}_i - \boldsymbol{r}_j$, $\hat{\boldsymbol{r}}_{ij} \equiv \boldsymbol{r}_{ij}/|\boldsymbol{r}_{ij}|$, $\boldsymbol{n}_{<ij>}$ is the unit normal vector of the bond $<ij>$ and the summations are over the vertices j connected to the vertex i by single bonds. Eq. (2–1) must be supplemented with the rules for topology change whenever a bond length shrinks to zero. There are two kinds of processes $T1$ and $T2$. The model is supposed to describe time evolution of two-dimensional cellular network in which the surface tension is the only driving force and the dissipation is associated with the motion of cell boundaries along their normal directions. In actual systems like soap bubbles, however, important dissipation arises from viscous flow of liquid within soap films near Platean borders (Kraynik, 1988), which is neglected here. Hence our present model does not describe any realistic situation. On the other hand, most studies of realistic models made unrealistic assumption of regular cellular structure (Kraynik, 1988), the only exception being that by Weaire and coworkers (Weaire and Kermode, 1984; Weaire and Fu, 1988). Thus, although our model is unrealistic for foam rheology, it has the virtue of dealing with irregular cellular structures. In the following, we describe two

kinds of computer simulations based on the vertex model.

3. Elastic and Plastic Properties

Since our vertex model defined in the proceeding section describes indefinite time evolution of cellular structure towards the state of lowest free energy consisting of a single cell, the model as it stands is not suitable for elasticity study. In order to avoid this difficulty we artificially impose the condition that after certain time area of every cell is fixed to be a constant (Kawasaki *et al.*, 1991). Physically this corresponds to supposing that transfer of incompressible fluid from one cell to another is completely stopped after a certain time. This condition can be readily incorporated by introducing a Lagrange multiplier λ_α for each cell α. The equation of motion is now written as

$$D\boldsymbol{v}_i = -\sum_j^{(i)} \hat{\boldsymbol{r}}_{ij} - \sum_\alpha^{(i)} \lambda_\alpha \frac{\partial A_\alpha}{\partial \boldsymbol{r}_i}, \tag{3-1}$$

where A_α is the area of the cell α and the sum in the second term is over the three cells which share the vertex i. See Appendix A for more details. Since in this section, we will be concerned only with stationary states, the left hand side of Eq. (3–1) is simplified where D is now a scalar constant.

The initial state of the simulation is prepared in the following way. First we take cellular patterns which are in the scaling regime after undergoing sufficient evolution in accordance with the model O equation of motion. We then let the system evolve according to the modified dynamics with constant cell areas where we monitor time variation of the free energy density $E(t)$ defined by

$$E(t) = \sum_{\langle ij \rangle} \left| \boldsymbol{r}_{ij}(t) \right| / A, \tag{3-2}$$

where A is the total area of the system. The sum is over all the pairs of vertices connected by single bonds. The run is continued until the system reaches an equilibrium defined by the following condition,

$$\left| E(t'+\delta t) - E(t') \right| / E(t') < 10^{-5} \quad \text{for} \quad t - 10\delta t \le t' \le t, \tag{3-3}$$

where δt is the size of a time step. This state is the initial state before distortion.

We now apply an elongational distortion by the following affine transformation

$$x(s+1) = e^{\varepsilon} x(s), \quad y(s+1) = e^{-\varepsilon} y(s), \tag{3-4}$$

where $x(s)$, $y(s)$ and $x(s+1)$, $y(s+1)$ are the coordinates of a material point before and after the transformation, respectively, and ε is the Hencky strain. Here s is a non-negative integer and $s = 0$ for the initial state. We then let the system evolve with the cell areas fixed until a new equilibrium state as defined by Eq. (3–3) is reached. By repeating the process we obtain the energy as a function of the total Hencky strain applied to the system.

The total number of cells in the initial state $s = 0$ was 493. The values of ε chosen were, $\varepsilon = 0.01$ for $0 \leq s \leq 79$ and $\varepsilon = -0.01$ for $80 \leq s \leq 159$. Some of the

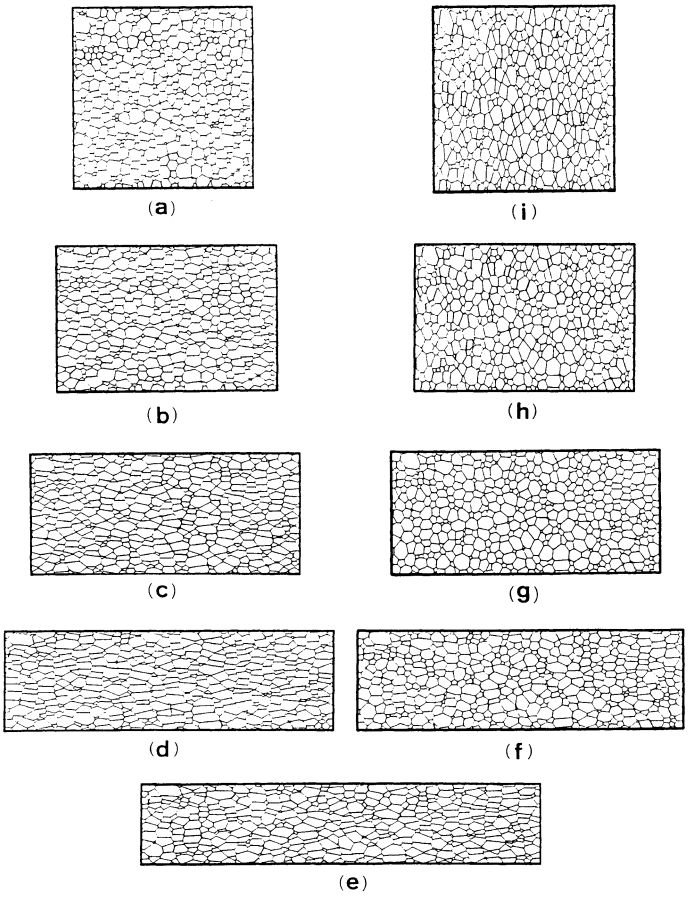

Fig. 1. Cellular patterns after successive deformations and equilibrations. The Hencky strains are (a) 0.0 (b) 0.2 (c) 0.4 (d) 0.6 (e) 0.8 (f) 0.6 (g) 0.4 (h) 0.2 (i) 0.0.

cell patterns during this deformation process are shown in Fig. 1. It is seen that a pattern depends not only on the accumulated deformation $\varepsilon_o(s)$ defined by εs for $0 \leq s \leq 80$ and $|\varepsilon|(160 - s)$ for $81 \leq s \leq 160$ but also on the past deformation history (hysteris effects). This is more clearly seen by the energy $E(t)$ written also as $E(s)$ or by the stress tensor $\tau_{\alpha\beta}$ defined by

$$\tau_{\alpha\beta} = -\frac{1}{A}\sum_{\langle ij \rangle} f_{ij}^{\alpha} r_{ij}^{\beta}, \tag{3-5}$$

where f_{ij} is the force acting along the bond $<ij>$ given by $-\hat{r}_{ij}$ for the vertex model. $E(s)$ is shown in Fig. 2 and $N_1(s) \equiv \tau_{xx}(s) - \tau_{yy}(s)$ is shown in Fig. 3. Figure 3 also shows the frequency of $T1$ processes during the course of deformation (more precisely, during each step $s - 1$ to s). These results show that for small enough deformation where no $T1$ process takes place the system behaves like an elastic solid, whereas at larger deformations where $T1$ processes occur the system shows plastic behavior in agreement with the indication of Ashby and Verral (1973). The topology changes are also responsible for the hysterisis effects.

We now note that besides the accumulated deformation one can also define the intrinsic deformation $\varepsilon_i(s)$ which reflects local changes of cell patterns rather than the system as a whole and is defined by

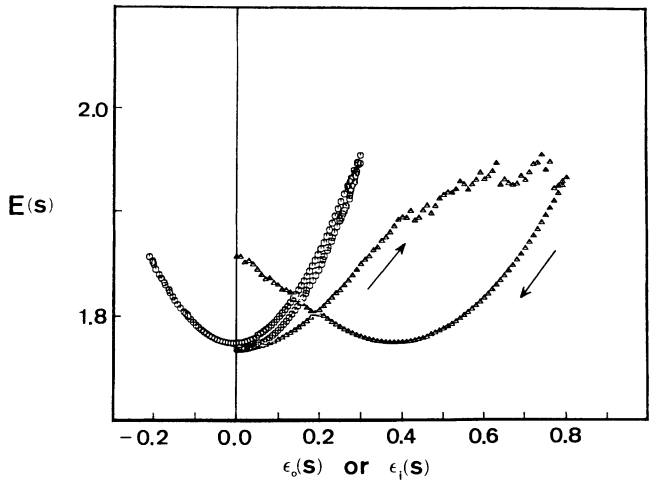

Fig. 2. Energy density plotted as a function of accumulated externally applied Hencky strain (Δ) and as a function of internal Hencky strain $\varepsilon_i(s)$(O). Arrows indicate directions of change.

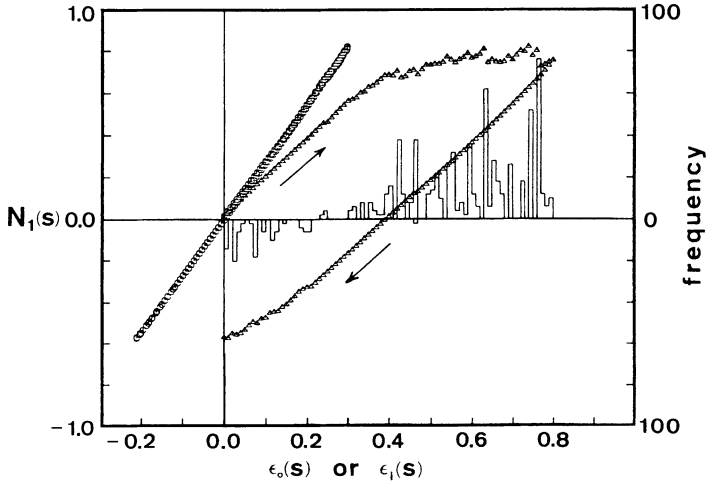

Fig. 3. Stress-strain relationship. The symbols are the same as in Fig. 2. Histograms show the frequency of $T1$ processes. Positive (negative) histograms are for increasing (decreasing) Hencky strains.

$$\varepsilon_i(s) = \frac{1}{2}\ln\left[l_x(s)/l_x(0)\right] - \frac{1}{2}\ln\left[l_y(s)/l_y(0)\right]. \qquad (3-6)$$

Here $l_\alpha(s)$ is the average linear size of a cell in the direction α at the time step s. See Appendix B for the precise definition. The results show in Figs. 2 and 3 also demonstrate that the system apparently behaves as an elastic body against intrinsic deformation with very little hysterisis effects. This is because the intrinsic deformation is a state variable independent of the past deformation history.

4. Viscoelastic Properties

We now return to the unconstrained dynamics of Section 2 and investigate the response of the system to the externally applied uniform rate of shear $\dot{\gamma}$ represented by the velocity field $\boldsymbol{u}(\boldsymbol{r})$ whose x and y-components are

$$u_x(\boldsymbol{r}) = \dot{\gamma}y, \; u_y(\boldsymbol{r}) = 0. \qquad (4-1)$$

The friction at the vertex i in the vertex model is assumed to be associated with the difference of $\boldsymbol{v}_i$ and $\boldsymbol{u}(\boldsymbol{r}_i)$ so that Eq. (2–1) is modified to

$$\boldsymbol{D}_i \cdot \left[\boldsymbol{v}_i - \boldsymbol{u}(\boldsymbol{r}_i)\right] = -\sum_j^{(i)} \hat{\boldsymbol{r}}_{ij}. \qquad (4-2)$$

Strictly speaking, the friction is associated with the difference of the velocity of an element of the cell boundaries and $\boldsymbol{u}$ at that point. However, the error should be negligible for sufficiently small velocity gradients. We simulated Eq. (4–2) using the Galilei-transformed periodic boundary condition. The initial state was chosen to be the matured state well in the scaling regime obtained using the original vertex equation of motion and contained $N_c(0) = 9628$ cells. The size of a time step δt was chosen to be $10^{-3}/\dot{\gamma}$ and the short bond length cut-off for topology change was taken to be $\Delta = 20\,\delta t$. Figure 4 shows shear stress $\tau_{xy}(t;\,\dot{\gamma})$ as a function of total strain $\dot{\gamma}\,t$ for different values of $\dot{\gamma}$. Here the units of time and length have been chosen to be $L^{-1}A/N_c(0)$ and $[A/N_c(0)]^{1/2}$, respectively where A and $N_c(0)$ are, respectively, the total system area and the total number of cells at the time zero. Fig. 5 shows the behavior of the transient shear viscosity defined by

$$\eta^{+}(t;\dot{\gamma}) = \tau_{xy}(t;\dot{\gamma})/\dot{\gamma}. \qquad (4-3)$$

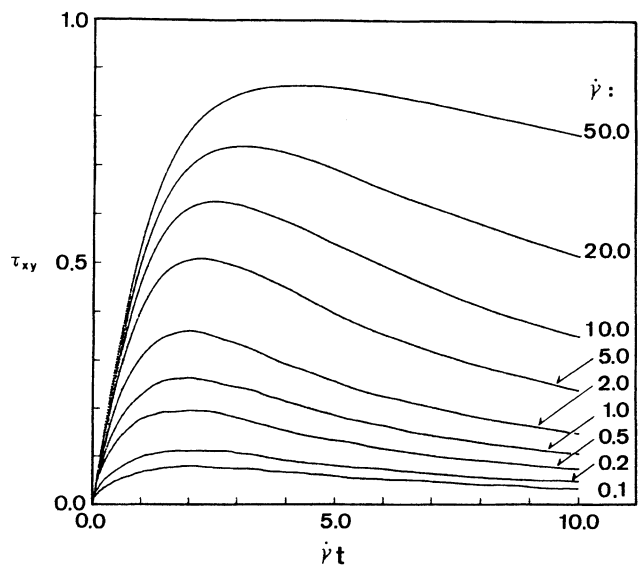

Fig. 4. Stress-strain relation for evolving cellular structures under shear for various shear rates.

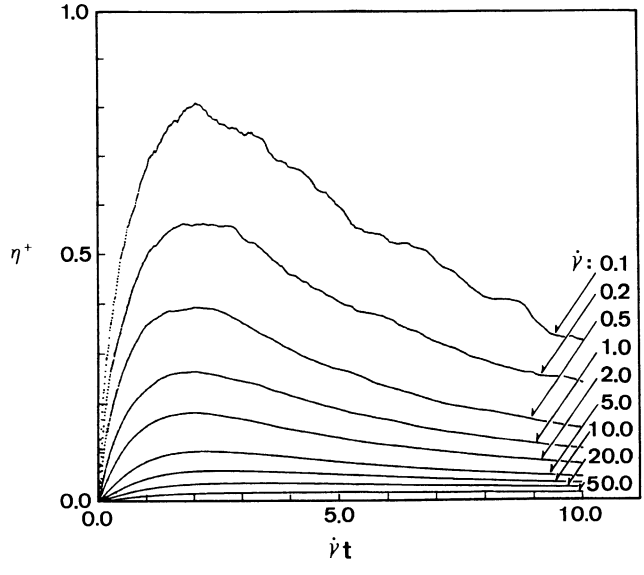

Fig. 5. Effective viscosity as a function of applied strain for various strain rates.

Both τ_{xy} and η^+ continue to decrease at largest values of $\dot{\gamma}\,t$ studied and a steady state is unlikely. Thus we examined the possibility of scaling behavior like

$$\tau_{xy}(t;\dot{\gamma}) = \dot{\gamma}^{\alpha}\,\tilde{\tau}_{xy}(\dot{\gamma}\,t). \qquad (4-4)$$

In Fig. 6 we plot $\dot{\gamma}^{-\alpha}\,\tau_{xy}(t;\dot{\gamma})$ as a function of $\dot{\gamma}\,t$ for five values of $\dot{\gamma}$ between 0.1 and 2.0. Here α is taken to be the average of the values obtained in the region $0.1 \leq \dot{\gamma} \leq 2.0$ and $2.0 \leq \dot{\gamma}\,t \leq 10.0$ and we find $\alpha = 0.496$. This value is very close to 0.5 obtained by the following dimensional consideration. From Eq. (3–5) $\tau_{\alpha\beta}$ scales as l^{-1}, l being the characteristic length of cellular pattern. For small $\dot{\gamma}$ we know that l grows as $t^{1/2}$. Now, $\dot{\gamma}$ has the dimension of t^{-1} and hence should scale as l^{-2}. Putting all these together we find that $\tau_{\alpha\beta}$ should scale as $\dot{\gamma}^{1/2}$ or $\alpha = 1/2$. This argument should be limited to small enough values of $\dot{\gamma}$ since the growth law $l \sim t^{1/2}$ is expected to be limited to small $\dot{\gamma}$. The break down of scaling occurs for $\dot{\gamma}$ between 2.0 and 5.0. We conjecture that the upper limit of $\dot{\gamma}$ will be given by the frequency of topology change per cell. Validity of this conjecture is suggested in Fig. 7 where the shear rate is compared with the average rate of topological change per cell for

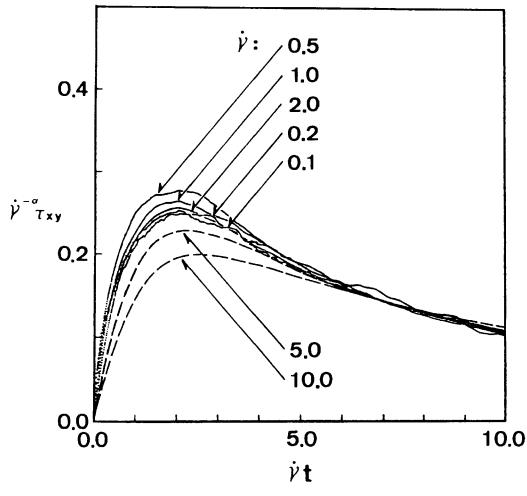

Fig. 6. Scaling behavior of stress-strain relationship.

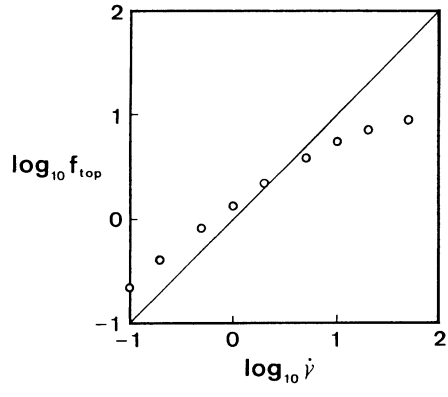

Fig. 7. Logarithmic plot of the average frequency of topology change per cell f_{top} (circles) and the rate of shear (straight line).

$0 \leq \dot{\gamma} t \leq 10$. We see that the value of $\dot{\gamma}$ where the scaling breaks down roughly coincides with the value of $\dot{\gamma}$ where the two rates are equal. We have also monitored the ratio of the frequencies of $T1$ and $T2$ processes and found that the ratio stays roughly constant at the value of 4 for the values of $\dot{\gamma}$ where scaling holds and begins to increase when the scaling starts to break down.

5. Discussion

Here we have demonstrated how the vertex models of cellular patterns can be used to study mechanical behavior of cellular structures including dynamical problem like viscoelasticity. However, there are much more to be desired for applications to real problems such as foam rheology. In foam rheology, for instance, the dissipation associated with fluid flow in liquid films into and out of Plateau borders is probably more important than that associated with transfer of air across liquid films (Kraynik, 1988). However, the experience gained with our simple vertex models should be quite useful in tackling more realistic models of cellular structures.

Acknowledgement

This work was supported in part by the Scientific Research Fund of the Ministry of Education, Science and Culture.

REFERENCES

Anderson, M. P. and Rollett, A. D., eds. (1990), Simulation and Theory of Evolving Microstructures (The Metallurgical Society, Warrendale, Pennsylvania).
Ashby, M. F. and Verrall, R. A., (1973), Acta Metall., **21**, 149.
Kawasaki, K., Nagai, T., and Okuzono, T. (1991), Microscopic Aspects of Nonlinearity in Condensed Matter, edited by A. R. Bishop *et al.* (Plenum Press, NY), 57–67.
Kraynik, A. M. (1988), Ann. Rev. Fluid Mech., **20**, 325–357.
Nagai, T. and Kawasaki, K. (1991), This volume.
Weaire, D. and Fu, T. L. (1988), J. Rheol., **32**, 271.
Weaire, D. and Kermode, J. P. (1984), Phil. Mag., **B50**, 379.
Weaire, D. and Rivier, N. (1984), Contemp. Phys., **25**, 59.

Appendix A

After some straightforward algebra, the Lagrange multipliers λ_α are shown to satisfy the following equation

$$\lambda_\alpha = -\left\{ 2\sum_{i}^{(\alpha)}\sum_{l}^{(i)} \hat{\boldsymbol{z}}\cdot\left(\boldsymbol{r}_{jk}\times\hat{\boldsymbol{r}}_{il}\right) + \sum_{\beta}^{(\alpha)}\left(\boldsymbol{r}_{jk}\cdot\boldsymbol{r}_{km}+\boldsymbol{r}_{li}\cdot\boldsymbol{r}_{im}\right)\lambda_\alpha \right\} \Big/ \sum_{i}^{(\alpha)} \boldsymbol{r}_{jk}^2, \quad (\mathrm{A}-1)$$

where $\hat{\boldsymbol{z}}$ is the unit vector directed upward from the two-dimensional system and the sums $\sum_i^{(\alpha)}$ and $\sum_\beta^{(\alpha)}$ are over the vertices belonging to the cell α and over the cells β adjoining the cell α, respectively. This is explained in Fig. 8. One can directly verify that the solution of Eq. (A–1) for λ_α is uniquely determined up to a common

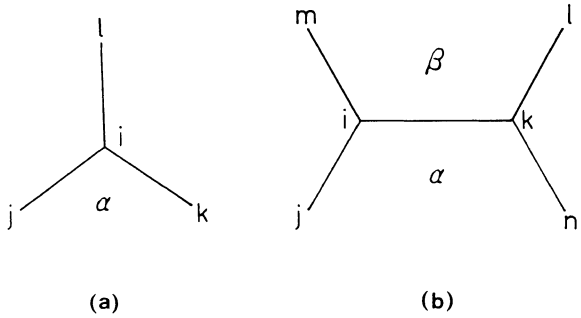

Fig. 8. Arrangement of vertices and cells for Eq. (A–1).

constant. Thus, if we impose another condition on λ_α like $\sum_\alpha \lambda_\alpha = 0$, the λ's can be uniquely determined.

Appendix B

l_α in Eq. (3–6) will be defined here. Let us draw a straight line parallel to the x-axis and count the number of its intersection with the bonds. Let n_x be this number divided by the total system length L_x along the x-axis averaged over many different straight lines along the x axis. Then l_x is defined by n_x^{-1}. l_y is then similarly defined. We can easily find

$$n_x = \frac{1}{L_x}\sum_{\langle ij\rangle}\frac{\left|r_{ij}^y\right|}{L_y} = \frac{1}{A}\sum_{\langle ij\rangle}\left|r_{ij}^y\right| \qquad (B-1)$$

and similarly for n_y.